GEOPHYSICS, VOL. 81, NO. 6 (NOVEMBER-DECEMBER 2016); P. D625–D641, 15 FIGS.
10.1190/GEO2016-0161.1

Bayesian linearized rock-physics inversion

Dario Grana[1]

ABSTRACT

The estimation of rock and fluid properties from seismic attributes is an inverse problem. Rock-physics modeling provides physical relations to link elastic and petrophysical variables. Most of these models are nonlinear; therefore, the inversion generally requires complex iterative optimization algorithms to estimate the reservoir model of petrophysical properties. We have developed a new approach based on the linearization of the rock-physics forward model using first-order Taylor series approximations. The mathematical method adopted for the inversion is the Bayesian approach previously applied successfully to amplitude variation with offset linearized inversion. We developed the analytical formulation of the linearized rock-physics relations for three different models: empirical, granular media, and inclusion models, and we derived the formulation of the Bayesian rock-physics inversion under Gaussian assumptions for the prior distribution of the model. The application of the inversion to real data sets delivers accurate results. The main advantage of this method is the small computational cost due to the analytical solution given by the linearization and the Bayesian Gaussian approach.

INTRODUCTION

In seismic reservoir characterization, the estimation of rock and fluid properties is generally achieved in two steps: seismic inversion and petrophysical (or rock-physics) inversion. In seismic inversion or elastic inversion (Russell, 1988), we invert the seismic data sets, i.e., amplitudes for different angle stacks, to estimate the elastic model, i.e., a 3D model of elastic attributes, such as P- and S-impedances, density, P- and S-wave velocities, and all the related seismic attributes. Seismic inversion can be performed using complex forward models and inverse algorithms, for example, full-waveform inversion and stochastic optimization, or using methods that are less computationally intense, such as seismic convolution and least-squares inversion. In petrophysical inversion (Doyen, 2007), we invert the seismic attributes obtained from seismic inversion to estimate a model of petrophysical properties, such as porosity, clay volume, and possibly fluid saturations. The petrophysical inversion requires a rock-physics model to link elastic and petrophysical properties (Mavko et al., 2009). This model is generally calibrated at the well location using well logs and/or laboratory measurements of core samples. The rock-physics model adopted in the inversion generally depends on the geologic environment. Granular media models based on Hertz-Mindlin contact theory are generally applied in reservoir with sand and shale formations, whereas inclusion models are often used in carbonate reservoirs (Avseth et al., 2005; Mavko et al., 2009; Dvorkin et al., 2014). If enough calibration data are available, empirical models such as the Han, Wyllie, and Raymer equations can be used as well. Most of the rock-physics models are generally nonlinear, except for the multilinear regressions proposed by Han (1986) for a data set in the Gulf of Mexico. Therefore, the inversion method requires nonlinear optimization algorithms, such as gradient-based methods, or stochastic optimization algorithms, such as genetic algorithms and simulated annealing (Doyen, 2007; Aster et al., 2011; Sen and Stoffa, 2013). Probabilistic approaches, such as Monte Carlo methods can be applied as well. One of the main advantages of a probabilistic approach is the assessment of the model uncertainty through the posterior distribution. However, the nonlinearity of the rock-physics model does not allow us to derive an analytical formulation for the posterior distribution of the petrophysical properties and requires the numerical estimation of the probability density function at each location of the reservoir.

A very common approach in inverse theory is Bayesian inversion, in which the prior distribution of the model is combined with the likelihood to observe the data given the model. In Bayesian inversion, if the forward model (hence the likelihood) is linear, the prior distribution is Gaussian, and the additive error term is Gaussian and independent of the model, then, the posterior distribution of the model given the measured data is also Gaussian, and the expressions for the conditional mean and conditional covariance matrix

Manuscript received by the Editor 28 March 2016; revised manuscript received 22 July 2016; published online 14 September 2016.
[1]University of Wyoming, Department of Geology and Geophysics, School of Energy Resources, Laramie, Wyoming, USA. E-mail: dgrana@uwyo.edu.

can be analytically derived (Tarantola, 2005). If the analytical solution is available, the computational cost of the inversion is very limited, compared with iterative optimization methods that require several evaluations of the objective function. Furthermore, the Gaussian assumption guaranties that the obtained solution minimizes the error in the least-square sense or l_2-norm (Tarantola, 2005).

In seismic inversion, Bayesian methods have been successfully applied for linearized seismic models, such as linearized amplitude variation with offset (AVO) inversion. Buland and Omre (2003) provide a seismic inversion algorithm based on the convolution (linear operator) of the wavelet and a linearized approximation of Zoeppritz equations (Aki and Richards, 1980). This method was also extended to time-lapse seismic inversion (Buland and El Ouair, 2006), Dix inversion (Buland et al., 2011), and CSEM inversion (Buland and Kolbjørnsen, 2012). The flexibility of the Bayesian approach also allows including a spatial model as in Buland et al. (2003) and Hansen et al. (2006). Furthermore, an unobservable discrete variable representing the lithofacies can be incorporated in the inversion as well (Larsen et al., 2006; Buland et al., 2008; Rimstad and Omre, 2010; Ulvmoen and Omre, 2010). Statistical sampling from the posterior distributions can be obtained by introducing a spatial correlation function in the inversion, or by combining the inversion results with more sophisticated geostatistical methods (Hansen et al., 2006; Doyen, 2007). Other statistical approaches have been presented by Mukerji et al. (2001), Mazzotti and Zamboni (2003), Eidsvik et al. (2004), Bornard et al. (2005), Coléou et al. (2005), Bachrach (2006), Gunning and Glinsky (2007), Spikes et al. (2007), González et al. (2008), Bosch et al. (2009), and Johansen et al. (2013). The Gaussian assumption is not necessarily required to achieve an analytical solution. Indeed, Grana and Della Rossa (2010) and Rimstad and Omre (2010) extend the Bayesian approach to Gaussian-mixture and generalized-Gaussian models, respectively. The main limitation of the applicability of the analytical Bayesian formulation to the rock-physics domain is the assumption that the model is linear. Bayesian approaches using nonparametric distributions and nonlinear models (e.g., based on kernel density estimation), have been proposed by Doyen (2007) for discrete properties (facies or lithofluid classes) and Grana and Della Rossa (2010) for petrophysical properties. However, the numerical evaluation of the posterior increases the computational cost, and the sampling algorithms are generally computationally demanding.

In this work, we propose to derive a linearization of the rock-physics model using first-order Taylor series approximations (Stewart, 2015). Using the proposed linearization and assuming a Gaussian prior model for the petrophysical properties, the solution of the inverse problem is represented by a Gaussian posterior distribution with explicit expressions for the posterior mean and covariance matrix. Analytical expressions for the confidence intervals are also available. This approach is valid for linear and almost linear rock-physics models. If the rock-physics model is strongly nonlinear, a piecewise linearization might be applicable. Otherwise, the proposed linearized approach cannot be applied, and a numerical evaluation of the posterior probability distribution is required.

Different from seismic inversion, in rock-physics inversion, the forward model depends on the rock type (Avseth et al., 2005; Mavko et al., 2009; Dvorkin et al., 2014). Several models are available in literature for different rock types. We can divide the models in three main categories: empirical, granular media, and inclusion models. For each category, we chose a specific model and derived the linearized Taylor approximation. In this work, we present the linearization of Raymer's equation, Dvorkin's stiff sand model, and the Kuster-Toksöz inclusion model (Mavko et al., 2009). We then present the analytical formulation of the posterior distribution of the Bayesian linearized rock-physics inversion. The accuracy of the inversion depends on the accuracy of the linearization of the rock-physics model. Although many rock-physics models are nonlinear, in the interval of interest (porosity between 0 and 0.5, mineral volumes and saturations between 0 and 1), these models are generally almost linear, and the linearization provides accurate approximations. Therefore, if the actual rock-physics model provides accurate elastic predictions (e.g., a good match of the sonic logs), then the linearization also provides good predictions. Three different applications are presented to illustrate the applicability of the method and the accuracy of the results.

METHODOLOGY

The inverse problem under study is the rock-physics inverse problem, i.e., the estimation of rock and fluid properties from seismic attributes. Examples of rock-physics inverse problems are the estimation of porosity and clay volume from P- and S-wave velocities in a clastic reservoir, or the estimation of porosity and water saturation from P-impedance and Poisson's ratio. If large offsets are available, and the density estimation from seismic data is reliable, then density could also be used as an input variable in the rock-physics inversion workflow.

In general, from a mathematical point of view, an inverse problem can be written in the form

$$d = f(m) + e, \tag{1}$$

where d represents the measured data at a given location, m is the model to be estimated, f is the physical relation that links the model to the data (the rock-physics model, in our case), and e is the measurement error associated with the data. We often assume the error to be Gaussian with zero mean and known standard deviation. In general, the error can follow any distribution, have nonzero mean, and be spatially correlated. For simplicity, we first assume that the variables are scalar and then extend the approach to the multivariate domain. For example, we can assume that d represents P-wave velocity, m is the porosity, and the rock-physics model is Raymer's equation.

The inverse problem in equation 1 is nonlinear because of the nonlinearity of the physical relation f. We then introduce a linearization based on the Taylor series expansion (Stewart, 2015). Taylor series expansions aim to approximate an arbitrary function at a given value of the independent variable using a polynomial in which the coefficients depend on the derivatives of the function. To correctly approximate the function, the series might contain infinite terms; however, for simple functions, a good approximation can be achieved using a limited number of terms. Taylor series are commonly used to study the behavior of numerical approximations to differential equations (Hörmander, 1990). For example, the forward Euler formula (Atkinson, 1989) corresponds to truncate the Taylor series after the second term. Taylor series have been previously used in geophysics to approximate complex nonlinear functions, especially in seismic imaging (see, e.g., Ursin and Stovas, 2006). In our approach, we are interested in linear approximations of rock-

physics models; therefore, the Taylor series expansion of the rock-physics equation is truncated after the first term. For the problem in equation 1, the first-order approximation is given by

$$d \cong f(m_0) + f'(m_0)(m - m_0) + e, \tag{2}$$

where f' is the first derivative of the function f and m_0 is a value of the independent variable m. In our application to inverse problems, we choose m_0 as the mean of the property. Given the limited range of the properties of interest in rock-physics inversion (porosity, mineral volumes, and fluid saturations), and the almost linear behavior of rock-physics models, this choice is not a limitation in many applications.

If we rearrange the terms in equation 2, then, we can reformulate the inverse problem as a linear inverse problem:

$$d \cong f'(m_0)m + (f(m_0) - m_0 f'(m_0)) + e = gm + b + e. \tag{3}$$

We now generalize this approach to a multivariate domain, in which the properties of interest (the data $\mathbf{d}$ and the model $\mathbf{m}$) are vectors of several variables. For example, $\mathbf{d}$ could represent P- and S-wave velocities and density and $\mathbf{m}$ could represent porosity, clay volume, and water saturation. By adopting a vector notation and applying a rock-physics model $\mathbf{f}$, the inverse problem can be written as

$$\mathbf{d} = \mathbf{f}(\mathbf{m}) + \mathbf{e} \tag{4}$$

The first-order Taylor series approximation is then

$$\mathbf{d} \cong \mathbf{f}(\mathbf{m_0}) + \mathbf{J}_{\mathbf{m_0}}(\mathbf{m} - \mathbf{m_0}) + \mathbf{e}, \tag{5}$$

where $\mathbf{J}_{\mathbf{m_0}}$ is the Jacobian of the function $\mathbf{f}$ evaluated at the point $\mathbf{m_0}$. The linearized inverse problem can then be rewritten as

$$\mathbf{d} \cong \mathbf{J}_{\mathbf{m_0}}\mathbf{m} + (\mathbf{f}(\mathbf{m_0}) - \mathbf{J}_{\mathbf{m_0}}\mathbf{m_0}) + \mathbf{e} = \mathbf{G}\mathbf{m} + \mathbf{b} + \mathbf{e}. \tag{6}$$

The additive constant $\mathbf{b}$ in equation 6 can be subtracted from the data $\mathbf{d}$, and the linear inverse problem can be written in the common form

$$\mathbf{d} - \mathbf{b} = \tilde{\mathbf{d}} = \mathbf{G}\mathbf{m} + \mathbf{e}. \tag{7}$$

If the rock-physics model can be written in the linear form as in equation 7, then the solution of the inverse problem can be obtained, in a Bayesian setting, with a relatively small computational cost.

If we assume that the model $\mathbf{m}$ is distributed according to a Gaussian distribution $N(\mathbf{m};\boldsymbol{\mu}_m, \boldsymbol{\Sigma}_m)$, the error is Gaussian with zero mean and covariance matrix $\boldsymbol{\Sigma}_e$, and the operator $\mathbf{f}$ is linear (with associated matrix $\mathbf{G}$), then the posterior distribution $p(\mathbf{m}|\mathbf{d})$ is also Gaussian $N(\mathbf{m};\boldsymbol{\mu}_{m|d}, \boldsymbol{\Sigma}_{m|d})$ and it can be analytically estimated through the following expressions for the conditional mean:

$$\boldsymbol{\mu}_{m|d} = \boldsymbol{\mu}_m + \boldsymbol{\Sigma}_m\mathbf{G}^T(\mathbf{G}\boldsymbol{\Sigma}_m\mathbf{G}^T + \boldsymbol{\Sigma}_e)^{-1}(\tilde{\mathbf{d}} - \mathbf{G}\boldsymbol{\mu}_m), \tag{8}$$

and for the conditional variance

$$\boldsymbol{\Sigma}_{m|d} = \boldsymbol{\Sigma}_m - \boldsymbol{\Sigma}_m\mathbf{G}^T(\mathbf{G}\boldsymbol{\Sigma}_m\mathbf{G}^T + \boldsymbol{\Sigma}_e)^{-1}\mathbf{G}\boldsymbol{\Sigma}_m. \tag{9}$$

The mathematical derivation of these expressions can be found in Tarantola (2005). The Bayesian approach can be extended to linear combinations of Gaussian distributions, i.e., Gaussian mixture models (Grana and Della Rossa, 2010). In the Gaussian mixture approach, we assume that a facies classification is available and that the prior model is a facies-dependent Gaussian distribution. The equations for the posterior mean and covariance matrix are the same as in equations 8 and 9, but the prior parameters $\boldsymbol{\mu}_m$ and $\boldsymbol{\Sigma}_m$ are facies dependent. The likelihood function, i.e., linear operator $\mathbf{G}$, can be either invariant or facies dependent. Rimstad and Omre (2010) also extend the analytical formulation, for seismic inversion, to generalized Gaussian models for analytical treatment of skewed distributions.

We point out that some empirical rock-physics models, such as Han's relations, are linear. Indeed, we can estimate the elastic attributes (velocities V_P, V_S and density ρ) as a function of petrophysical properties (porosity ϕ, clay volume C, and water saturation S_w) using a multilinear regression

$$\begin{cases} V_P = \alpha_P\phi + \beta_P C + \gamma_P S_w + \delta_P, \\ V_S = \alpha_S\phi + \beta_S C + \gamma_S S_w + \delta_S, \\ \rho = \alpha_R\phi + \beta_R C + \gamma_R S_w + \delta_R, \end{cases} \tag{10}$$

and rewrite the rock-physics model in the matrix form

$$\begin{bmatrix} V_P \\ V_S \\ \rho \end{bmatrix} = \begin{bmatrix} \alpha_P & \beta_P & \gamma_P \\ \alpha_S & \beta_S & \gamma_S \\ \alpha_R & \beta_R & \gamma_R \end{bmatrix} \begin{bmatrix} \phi \\ C \\ S_w \end{bmatrix} + \begin{bmatrix} \delta_P \\ \delta_S \\ \delta_R \end{bmatrix}. \tag{11}$$

This case does not require any additional linearization. In the following, we show how to linearize some common rock-physics models: the Raymer et al. (1980) model, the Dvorkin et al. (1994) stiff sand model, and the Kuster and Toksöz (1974) inclusion model.

Linearized Raymer model

Raymer proposes to estimate P-wave velocity V_P as a quadratic function of porosity ϕ (Raymer et al., 1980). Raymer's equation depends on the P-wave velocity of the solid phase $V_{P,mat}$ and the P-wave velocity of the fluid phase $V_{P,fl}$, which depend, respectively, on the clay volume C (assuming a mixture of quartz and clay) and the water saturation S_w (assuming a mixture of brine and hydrocarbon). Dvorkin later extends Raymer's model to S-wave velocity prediction as a function of porosity ϕ, S-wave velocity in the solid phase $V_{S,mat}$, and density ρ (Dvorkin, 2008). Finally, density can be computed as a linear average of porosity in which the coefficients depend on the density of the solid phase ρ_{mat} and the density of the fluid phase ρ_{fl}. By combining Raymer, Raymer-Dvorkin, and the density equation, we obtain a system of three equations in three unknowns (porosity ϕ, clay volume C, and water saturation S_w)

$$\begin{cases} V_P = (1-\phi)^2 V_{P,mat} + \phi V_{P,fl}, \\ V_S = (1-\phi)^2 V_{S,mat}\sqrt{\frac{(1-\phi)\rho_{mat}}{\rho}}, \\ \rho = (1-\phi)\rho_{mat} + \phi\rho_{fl}, \end{cases} \tag{12}$$

where

$$\rho_{\text{mat}} = \rho_c C + \rho_q (1 - C), \tag{13}$$

$$\rho_{\text{fl}} = \rho_w S_w + \rho_{hc}(1 - S_w), \tag{14}$$

$$V_{\text{P,mat}} = \sqrt{\frac{K_{\text{mat}} + \frac{4}{3} G_{\text{mat}}}{\rho_{\text{mat}}}}, \tag{15}$$

$$V_{\text{S,mat}} = \sqrt{\frac{G_{\text{mat}}}{\rho_{\text{mat}}}}, \tag{16}$$

$$V_{\text{P,fl}} = \sqrt{\frac{K_{\text{fl}}}{\rho_{\text{fl}}}}, \tag{17}$$

and

$$K_{\text{mat}} = \frac{(CK_c + (1 - C)K_q) + \left(\frac{1}{C/K_c + (1-C)/K_q}\right)}{2}, \tag{18}$$

$$G_{\text{mat}} = \frac{(CG_c + (1 - C)G_q) + \left(\frac{1}{C/G_c + (1-C)/G_q}\right)}{2}, \tag{19}$$

$$K_{\text{fl}} = S_w K_w + (1 - S_w)K_{hc}, \tag{20}$$

where K and G are the bulk and shear moduli, respectively. The subscript hc indicates hydrocarbon (oil or gas), w indicates water, c indicates clay, and q indicates quartz. In particular, the densities of solid and fluid are computed as a weighted average of the mineral and fluid components (equations 13 and 14), the P- and S-wave velocities of the solid phase are computed using the Voigt-Reuss-Hill average for the solid bulk and shear moduli (equations 18 and 19), and the velocity of the fluid phase is computed using the Voigt average for the fluid bulk modulus (equation 20). The Voigt average for the fluid mixture is generally suitable for patchy saturation systems; alternatively, Brie's relation could be used as well (Mavko et al., 2009). If the fluid mixture is homogeneous, the Reuss average should be used:

$$K_{\text{fl}} = \frac{1}{S_w/K_w + (1 - S_w)/K_{hc}}. \tag{21}$$

To derive the linearization of the rock-physics model in equation 12, we first compute the Jacobian

$$\boldsymbol{J}(\phi, C, S_w) = \begin{bmatrix} \frac{\partial V_{\text{P}}}{\partial \phi} & \frac{\partial V_{\text{P}}}{\partial C} & \frac{\partial V_{\text{P}}}{\partial S_w} \\ \frac{\partial V_{\text{S}}}{\partial \phi} & \frac{\partial V_{\text{S}}}{\partial C} & \frac{\partial V_{\text{S}}}{\partial S_w} \\ \frac{\partial \rho}{\partial \phi} & \frac{\partial \rho}{\partial C} & \frac{\partial \rho}{\partial S_w} \end{bmatrix}. \tag{22}$$

The partial derivatives are shown in Appendix A. To obtain the linearization of the rock-physics model in equation 12, we evaluate the Jacobian of the function (Appendix A) at a given point of the model space, for example, $\mathbf{m_0} = [\mu_\phi, \mu_C, \mu_{S_w}]$ with μ being the variable mean; we evaluate the rock-physics model (equation 12) at the same point $\mathbf{m_0}$; and we derive the first-order Taylor series approximation as in equation 6. In Figure 1, we show the comparison between the exact rock-physics model and the linearized approximation. To compute the actual model, we assumed two mineral components, clay and quartz, and two fluid components, oil and water, and the following parameters: $K_c = 21$ GPa, $G_c = 15$ GPa, $\rho_c = 2.45$ g/cm^3, $K_q = 36$ GPa, $G_q = 36$ GPa, $\rho_q = 2.65$ g/cm^3, $K_{hc} = 0.8$ GPa, $\rho_{hc} = 0.6$ g/cm^3, $K_w = 2.25$ GPa, and $\rho_w = 1.03$ g/cm^3. In this example, we assume a patchy fluid mixture (equation 20). In Figure 1a and 1b, we notice that the linearized model approximates the rock-physics model very well for intermediate porosities but tends to underestimate the model for low- and high-porosity values. When the model is extended to the entire reservoir, the mismatch could lead to misclassifications. To improve the approximate model, we propose a piece-wise linearized model. We first define a set of lithologic facies and then compute the model linearization in each facies. In this example, for simplicity, we define three facies: low-porosity (corresponding to the porosity interval [0–0.1]), mid-porosity (interval [0.1–0.2]), and high-porosity facies (interval [0.2–0.3]). In real studies, facies might be defined based on multiple properties (for example, porosity and clay volume) and sedimentological models.

The piecewise linearized model is shown in Figure 2a and 2b shows an improvement of the approximation for low and high porosity values. Figure 2c and 2d also illustrates a case in which the linearization might fail. The mineralogical model is the same as in Figure 1, but the fluid mixture is a homogeneous mixture of gas ($K_{hc} = 0.1$ GPa, $\rho_{hc} = 0.1$ g/cm^3) and water. The velocity of the fluid phase in the Raymer equation is then computed using the Reuss average (equation 21). The harmonic average for the fluid bulk modulus introduces a nonlinearity in the rock-physics model and the linearization fails for high values of water saturation. Indeed, a small amount of gas results in a large decrease in the P-wave velocity, whereas a further increase in gas saturation has smaller effects. Therefore, in such a situation, a linearized inversion might introduce misclassifications of the fluid content in the reservoir.

Linearized stiff sand model

The stiff sand model is based on Hertz-Mindlin equations and the modified Hashin-Shtrikman upper bounds (Dvorkin et al., 2014). Hertz-Mindlin grain-contact theory provides an estimation of the bulk and shear moduli of a dry rock, under the assumption that the rock frame is a random pack of spherical grains, subject to an effective pressure P_e, with a given porosity ϕ_c, and an average number of contacts per grain n (coordination number). In the stiff sand model, Hertz-Mindlin equations are used to compute the values of the dry-rock elastic moduli K_{HM} and G_{HM} at the critical porosity ϕ_c. The values of the elastic moduli of the solid phase K_{mat} and G_{mat} (i.e., the elastic moduli at zero porosity) can be computed using Voigt-Reuss-Hill average. The stiff sand model provides an estimate of the dry-rock elastic moluli, K_{dry} and G_{dry}, for all the porosity values within the porosity range $[0, \phi_c]$ by interpolating the elastic moduli at zero porosity (K_{mat} and G_{mat}) and the elastic moduli at the critical porosity (K_{HM} and G_{HM}) using the modified Hashin-Shtrikman upper bounds (Dvorkin et al., 2014):

$$K_{\text{dry}} = \left(\frac{\phi/\phi_c}{K_{\text{HM}} + 4/3G_{\text{mat}}} + \frac{1-\phi/\phi_c}{K_{\text{mat}} + 4/3G_{\text{mat}}}\right)^{-1} - \frac{4}{3}G_{\text{mat}}, \tag{23}$$

$$G_{\text{dry}} = \left(\frac{\phi/\phi_c}{G_{\text{HM}} + \xi} + \frac{1-\phi/\phi_c}{G_{\text{mat}} + \xi}\right)^{-1} - \xi, \tag{24}$$

where

$$\xi = \frac{1}{6}G_{\text{mat}}\frac{9K_{\text{mat}} + 8G_{\text{mat}}}{K_{\text{mat}} + 2G_{\text{mat}}}. \tag{25}$$

To include the fluid effect, we combine the stiff sand model with Gassmann's equations and obtain the saturated-rock elastic moduli K_{sat} and G_{sat}. According to Gassmann's equations, the saturated-rock bulk modulus K_{sat} is a function of porosity, rock and fluid elastic moduli, and dry-rock bulk modulus K_{dry}, whereas the saturated-rock shear modulus G_{sat} is equal to the dry-rock shear modulus G_{dry}. For the fluid bulk modulus, we assume the Voigt average as in the previous model (equation 20). Finally, velocities V_{P} and V_{S} are computed as a function of the elastic moduli and density:

$$V_{\text{P}} = \sqrt{\frac{M_{\text{sat}}}{\rho}} = \sqrt{\frac{K_{\text{sat}} + 4/3G_{\text{sat}}}{\rho}}, \tag{26}$$

$$V_{\text{S}} = \sqrt{\frac{G_{\text{sat}}}{\rho}}, \tag{27}$$

where $M_{\text{sat}} = K_{\text{sat}} + 4/3G_{\text{sat}}$ is the compressional modulus of the saturated rock and $\rho = (1-\phi)\rho_{\text{mat}} + \phi\rho_{\text{fl}}$ is the density.

The challenge of the linearization of the stiff sand model is in the computation of the derivatives to form the Jacobian. In the following, we assume that the clay volume is constant; therefore, K_{mat} and G_{mat} are constant. We also assume that the coordination number, the critical porosity, and the pressure are constant parameters; therefore, the Hertz-Mindlin elastic moduli at the critical porosity, K_{HM} and G_{HM}, are constant as well. Using a mathematical software, the computation of the Jacobian of the model with variable clay volume is also possible. Otherwise, a facies classification can be preliminarily computed, and an average value for the solid properties can be assigned to each facies. The partial derivatives are shown in Appendix B. The linearization is obtained through equation 6. In Figure 3, we show the comparison between the exact rock-physics model and the linearized approximation. To compute the actual model, we made the same assumptions as in the Raymer model. We also assumed that the critical porosity is 0.4, the coordination number is 7, and the effective pressure is 20 MPa. The elastic moduli of the solid phase are computed using Voigt-Reuss-Hill averages. Due to the almost linear behavior of the rock-physics model with respect to porosity, the linearized model matches the exact model very well.

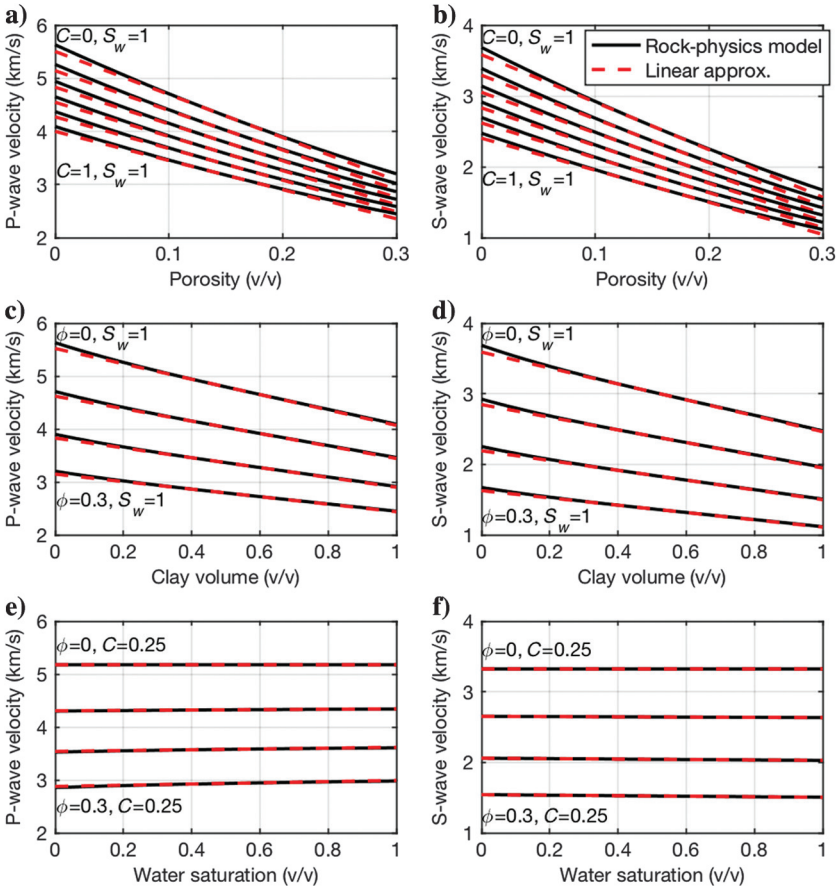

Figure 1. Raymer model: comparison between exact rock-physics model (solid black lines) and linear approximation (dashed red lines). Top plots: (a) P-wave velocity and (b) S-wave velocity versus porosity (clay volume varies from 0 to 1 with steps of 0.2, water saturation is assumed to be constant and equal to one); mid plots: (c) P-wave velocity and (d) S-wave velocity versus clay volume (porosity varies from 0 to 0.3 with steps of 0.1, water saturation is assumed to be constant and equal to one); and bottom plots: (e) P-wave velocity and (f) S-wave velocity versus water saturation (porosity varies from 0 to 0.3 with steps of 0.1; clay volume is assumed to be constant and equal to 0.25).

Similar results can be obtained for clay content and water saturation (assuming a patchy saturation mixture).

Linearized inclusion model

The Kuster and Toksöz (1974) inclusion model is a rock-physics model used to estimate the elastic properties of dry and saturated rocks by using first-order scattering theory. Several formulations have been proposed (Mavko et al., 2009). In our work, we assume that the mineral phase is homogeneous (i.e., the elastic moduli K_{mat}, G_{mat}, and M_{mat} are constant values), and we use the following formulation to compute the elastic moduli of the saturated rock:

$$(K_{sat} - K_{mat})\frac{M_{mat}}{K_{sat} + \frac{4}{3}G_{mat}} = \phi(K_{fl} - K_{mat})P, \tag{28}$$

$$(G_{sat} - G_{mat})\frac{G_{mat} + \xi}{G_{sat} + \xi} = -\phi G_{mat}Q, \tag{29}$$

where P and Q are the geometric factors and K_{fl} and ξ are given in equations 20 and 25, respectively. For solid mixtures, the elastic moduli, K_{mat} and G_{mat}, can be computed using Voig-Reuss-Hill averages (equations 18 and 19). Different geometric shapes can be used for the inclusions, such as spheres and ellipsoids. For simplicity, we assume spherical inclusions; therefore, the expressions for the geometric factors are given by

$$P = \frac{K_{mat} + \frac{4}{3}G_{mat}}{K_{fl} + \frac{4}{3}G_{mat}}, \tag{30}$$

$$Q = \frac{G_{mat} + \xi}{\xi}. \tag{31}$$

The expressions for ellipsoids are more complex and depend on an additional parameter, namely the aspect ratio (Mavko et al., 2009). To compute the Jacobian of the model in equations 28 and 29, we first explicitly write the saturated-rock elastic moduli, and we substitute the expressions for the geometric factors. After simplification, we obtain the following expressions:

$$K_{sat} = \frac{4K_{mat}G_{mat} + 3K_{mat}K_{fl} + 4G_{mat}K_{fl}\phi - 4K_{mat}G_{mat}\phi}{4G_{mat} + 3K_{fl} - 3K_{fl}\phi + 3K_{mat}\phi}, \tag{32}$$

$$G_{sat} = \frac{G_{mat}(9K_{mat} + 8G_{mat})(1 - \phi)}{9K_{mat} + 8G_{mat} + 6(K_{mat} + 2G_{mat})\phi}. \tag{33}$$

We then compute the velocities as a function of the elastic moduli K_{sat} and G_{sat} and density $\rho = (1 - \phi)\rho_{mat} + \phi\rho_{fl}$. The partial derivatives are shown in Appendix C. The linearization is obtained through equation 6. A similar formulation can be obtained for other inclusion shapes, such as needles, disks, and penny cracks (Mavko et al., 2009); however, the expressions of the derivatives become more complex and should be obtained using a mathematical software. Similarly, the proposed formulation can be extended to include multiple mineral volumes. In Figure 4, we present the comparison between the exact rock-physics model and the linearized approximation, showing a good match.

APPLICATION

We present here the application of the Bayesian linearized rock-physics inversion to a real data set from an oil reservoir in the North Sea. The data set includes a set of well logs (P- and S-wave velocities and density) and computed properties (effective porosity, clay volume, and water saturation) and a 2D inverted seismic line across the well. The elastic logs and computed petrophysical parameters are shown in Figure 5. The main reservoir layer is characterized by approximately 20 m of clean sand with low percentages of clay and with oil saturation close to 90%, followed by a sequence of thin oil-sand layers alternated to interbedded shaley layers. The layers

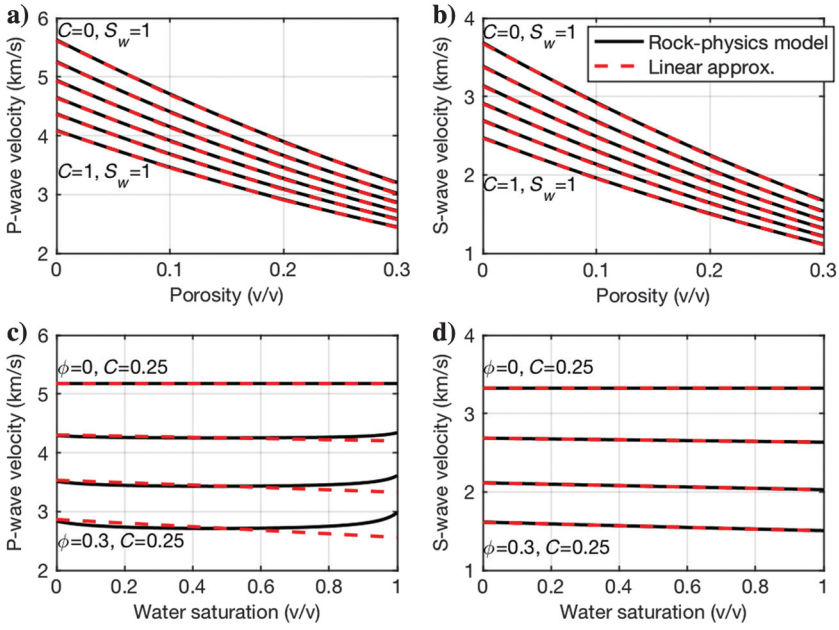

Figure 2. Raymer model: comparison between exact rock-physics model (solid black lines) and linear approximation (dashed red lines). Top plots show the piecewise linearization: (a) P-wave velocity and (b) S-wave velocity versus porosity (clay volume varies from 0 to 1 with steps of 0.2, water saturation is assumed to be constant and equal to one). Bottom plots show the linearization for homogeneous mixtures of gas and water: (c) P-wave velocity and (d) S-wave velocity versus water saturation (porosity varies from 0 to 0.3 with steps of 0.1; clay volume is assumed to be constant and equal to 0.25).

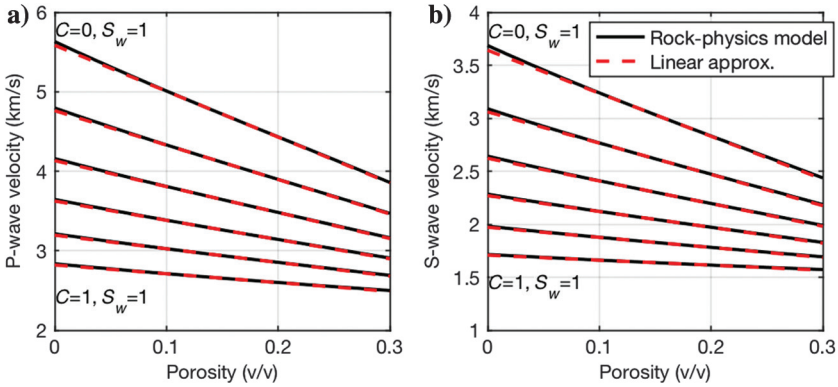

Figure 3. Stiff sand model: comparison between exact rock-physics model (solid black lines) and linear approximation (dashed red lines). Plots show (a) P-wave velocity and (b) S-wave velocity versus porosity (clay volume varies from 0 to 1 with steps of 0.2; water saturation is assumed to be constant and equal to one).

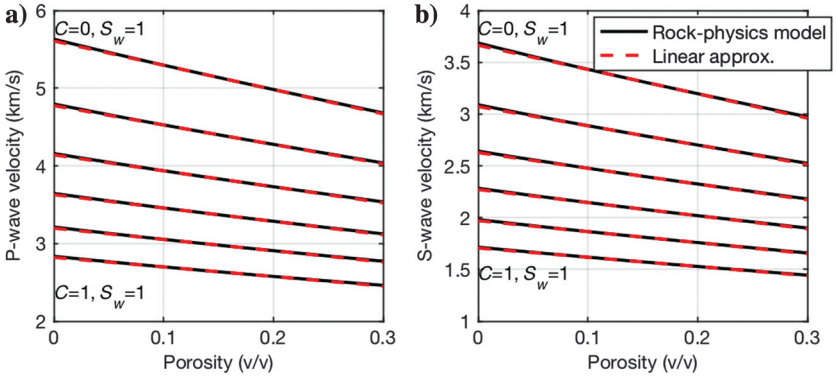

Figure 4. Inclusion model: comparison between exact rock-physics model (solid black lines) and linear approximation (dashed red lines). Plots show (a) P-wave velocity and (b) S-wave velocity versus porosity (clay volume varies from 0 to 1 with steps of 0.2; water saturation is assumed to be constant and equal to one).

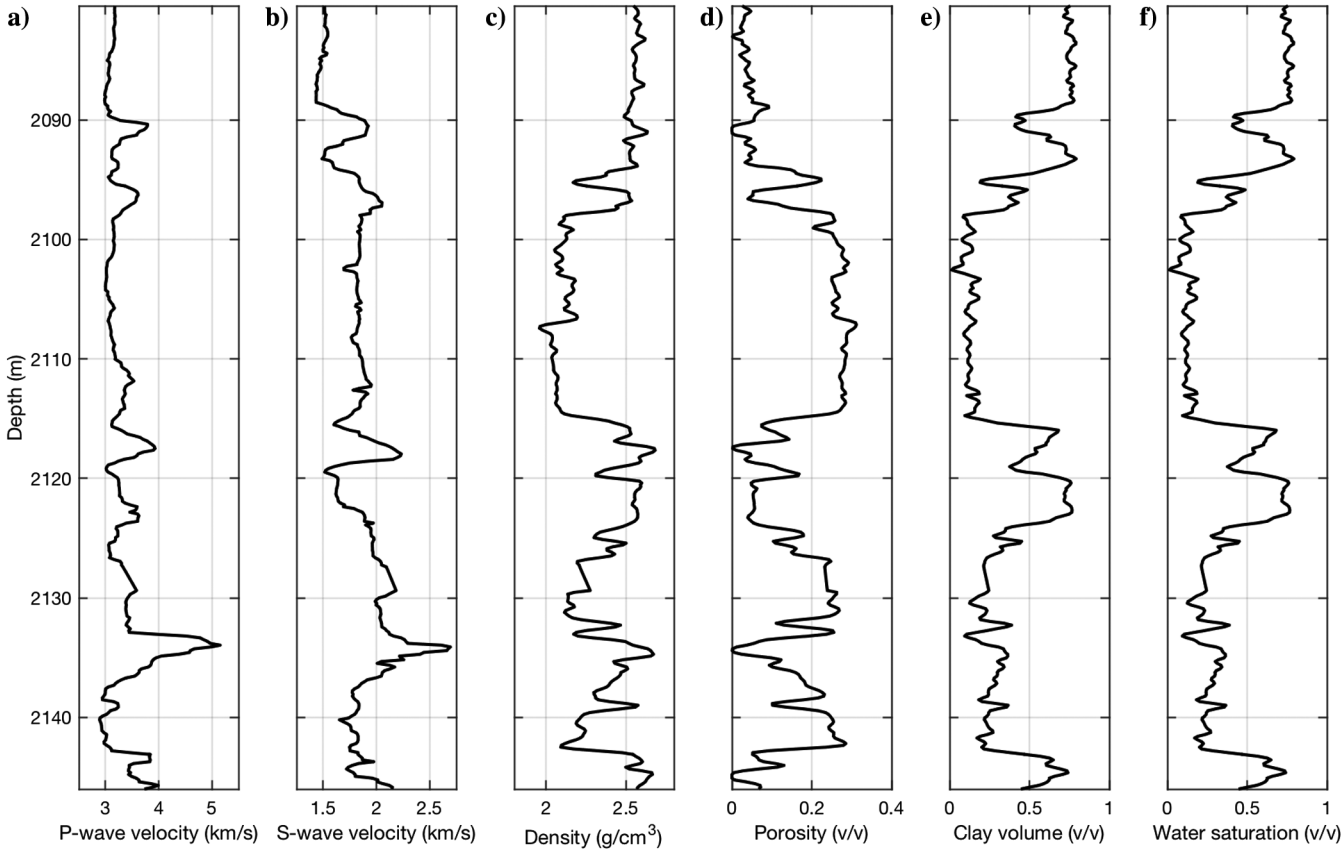

Figure 5. Well-log data set including elastic logs and computed petrophysical parameters. (a) P-wave velocity, (b) S-wave velocity, (c) density, (d) effective porosity, (e) clay volume, and (f) water saturation.

above and below the reservoir mostly contain clay. The application is divided into two parts: in the first part, we aim to estimate the model parameters (namely, effective porosity, clay volume, and water saturation) from the measured log data (P- and S-wave velocities and density); in the second part, we extend the inversion to the 2D section of inverted seismic attributes.

In the first part of the application, we calibrate the rock-physics model to fit the log measurements, and we compare the results of three different models: Raymer, stiff sand, and inclusion model. The relations between petrophysical and elastic properties are shown in Figure 6, in which we superimpose Raymer and Raymer-Dvorkin models to the well-log measurements. The model curves are computed for different values of clay volume ranging from 0.05 to 0.8 (with step 0.15) and compared with log measurements. Figure 7 shows the rock-physics model predictions (Raymer model) at the well location using the exact model (red lines) and the linearized model (dashed blue lines) for P- and S-wave velocities and density. The exact and linearized models approximate the elastic logs. The average errors between the linearized model and the actual elastic logs are approximately 6.1% for P-wave velocity, 7.2% for S-wave velocity, and 2.5% for density. A few layers (at depths 2118, 2129, and 2134 m) show mismatches with errors between 15% and 18%. These layers might correspond to interbedded carbonate layers not accounted for in formation-evaluation analysis, measurements

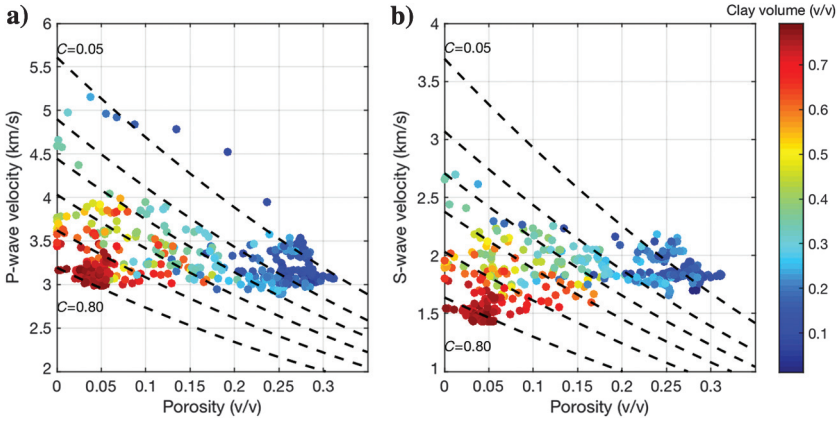

Figure 6. Rock-physics model calibration (Raymer-Dvorkin model): (a) P-wave velocity versus porosity and (b) S-wave velocity versus porosity. Log measurements are color coded by clay volume. Black curves represent (a) Raymer model and (b) Raymer-Dvorkin model for six values of clay volume (from top to bottom, the clay volume is 0.05, 0.20, 0.35, 0.50, 0.65, and 0.8).

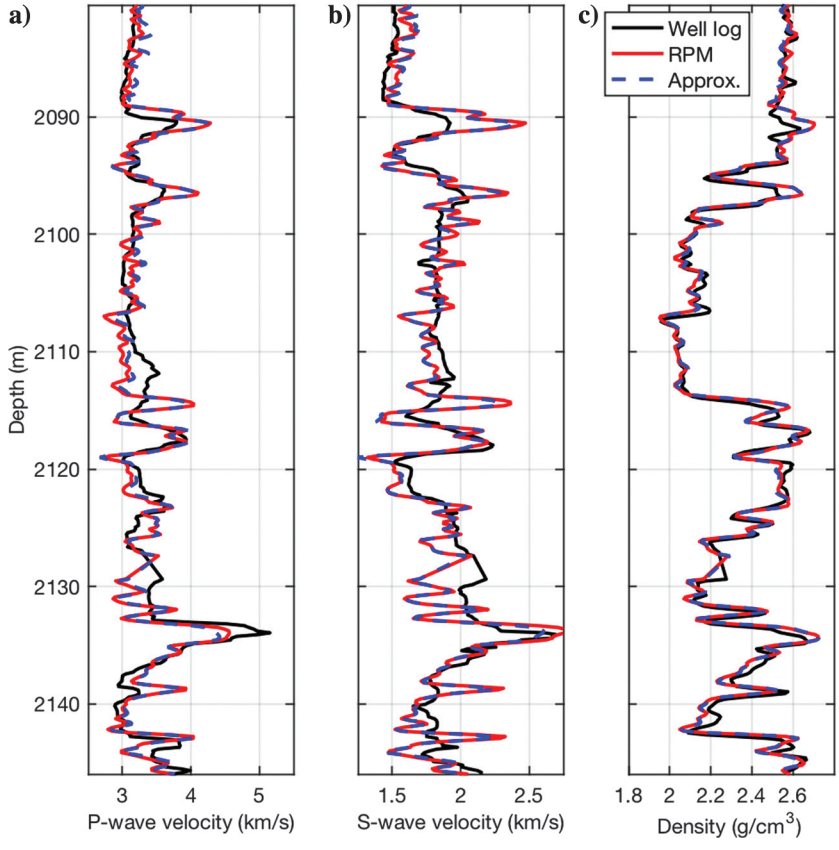

Figure 7. Rock-physics model approximation (Raymer-Dvorkin model). (a) P-wave velocity, (b) S-wave velocity, and (c) density (black curves represent the actual well log, red curves represent the rock-physics model predictions, and dashed blue curves represent the linearized model predictions).

errors, misalignments of elastic and petrophysical logs, or incorrect well-log interpretation and mineralogical analysis. As expected, the density predictions show a very good match with the density log.

We then apply the Bayesian rock-physics inversion using the linearized model. The aim of the inversion is to estimate the posterior probability distribution of the petrophysical properties (effective porosity, clay volume, and water saturation) given the elastic attributes (P- and S-wave velocities and density). For the prior distribution of the petrophysical properties, we assume a trivariate Gaussian distribution. The prior distribution is spatially invariant. The marginal distribution of porosity is $N(\phi; 0.15, 0.01)$, the marginal distribution of clay volume is $N(C; 0.39, 0.06)$, and the marginal distribution of water saturation is $N(S_w; 0.56, 0.14)$. The marginal distributions are shown in Figure 8. We assume a prior correlation between porosity and clay volume of -0.8, a prior correlation between clay volume and water saturation of 0.8, and a prior correlation between porosity and water saturation of -0.8. We point out that a Gaussian mixture distribution might be more appropriate for this application, given the bimodality of the data; however, for simplicity, we assume a Gaussian prior. We also assume a Gaussian distribution with zero mean and spatially invariant covariance matrix for the error term. The covariance matrix of the error is assumed to be diagonal with variances equal to 5% of the mean of the actual data measurements (i.e., 5% of the mean of P-wave velocity, 5% of the mean of S-wave velocity, and 5% of the mean of density). The inversion is first applied to elastic log data to compare the results with the actual petrophysical curves of porosity, clay volume, and water saturation. At each depth location in the well log, we compute the posterior distribution of porosity, clay volume, and water saturation conditioned by P- and S-wave velocities and density. The posterior distributions are truncated at the boundaries of the petrophysical property ranges to avoid nonphysical values, and the probability density exceeding the physical boundaries is redistributed within the physical range. The results for the Raymer model are shown in Figure 8. Overall, the probability distributions capture the trend of the actual logs. The posterior standard deviation of porosity is reduced by 42% compared with the prior, the standard deviation of clay volume is reduced by 45%, and the standard deviation of water saturation by 46%. Given the good match between the actual rock-physics model and the linearized approximation, we point out that the misclassifications in the posterior probability distributions are due to the lack of accuracy of the original rock-physics model.

We then repeat the inversion using the stiff sand model (Figures 9 and 10) and the inclusion model (Figures 11 and 12). The linearization shown in Appendices B and C assume a constant clay volume. In this application, we extended the model to variable clay content using a mathematical software to compute the derivatives. The stiff sand model and its linear approximation are shown in Figure 9. Because the model tends to overestimate S-wave velocity,

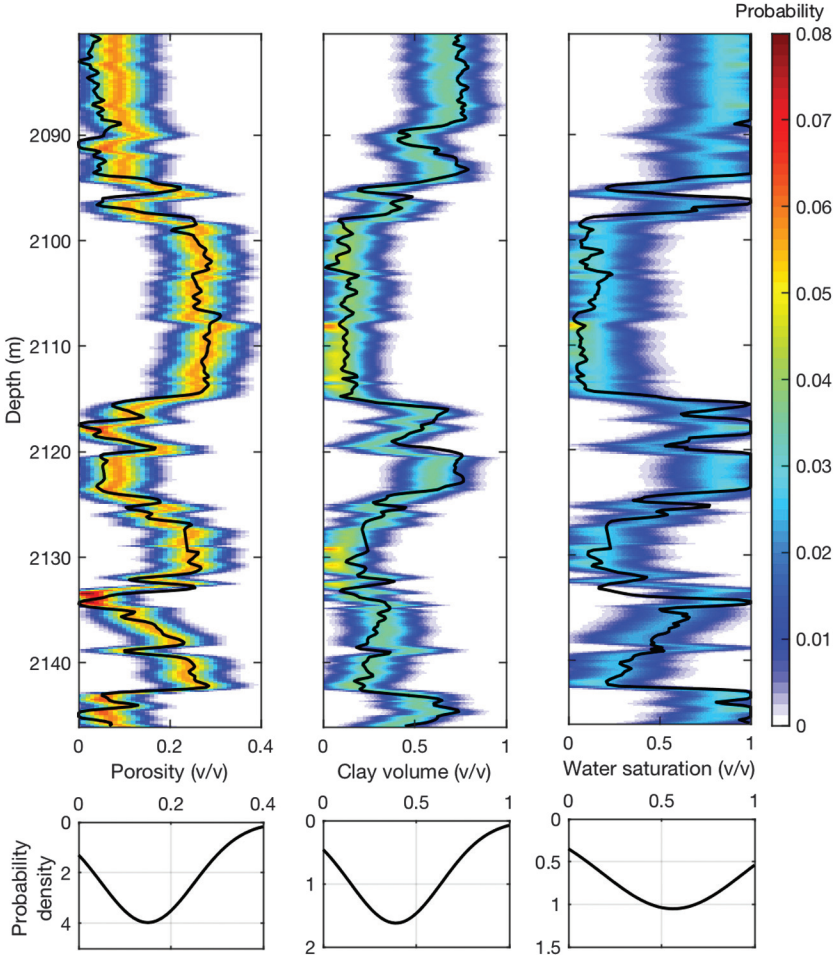

Figure 8. Rock-physics model inversion of elastic-log data (Raymer-Dvorkin model). From left to right: posterior probability distributions of porosity, clay volume, and water saturation (black lines represent the actual well data, and the background color represents the posterior probability distribution). The bottom plots show the prior marginal distributions of porosity, clay volume, and water saturation, respectively.

we decreased the value of the shear modulus of the solid phase to match the well-log data. The linearized model approximates the actual rock-physics model well. For the inversion, we assume the same trivariate Gaussian distribution for the model parameters. We then estimate the posterior marginal probability of porosity, clay volume, and water saturation conditioned by elastic properties. The prior and posterior probability distributions are shown in Figure 10.

Finally, we calibrate the inclusion model and invert the elastic-log data assuming the same prior model as in the previous examples. The rock-physics model calibration is shown in Figure 11. The velocity estimations are similar to the stiff sand model predictions. The prior and marginal posterior distributions of porosity, clay volume, and water saturations are shown in Figure 12. In all the examples, namely, the Raymer, stiff sand, and inclusion models, the uncertainty on the posterior distribution is reduced compared with the prior uncertainty.

The linearized rock-physics inversion can then be extended to the entire reservoir volume. In the second part of the study, we apply the Bayesian inversion approach to a set of inverted seismic attributes (P- and S-wave velocities and density) along a seismic crossline (Figure 13). Seismic attributes were obtained through a deterministic elastic inversion based on a convolutional approach. The well is located at location 2750 m according to the relative scale of the crossline (Figure 13). The rock-physics model used for the inversion is the Raymer model calibrated to well-log data (Figures 6 and 7). The elastic properties along the 2D section show low resolution due to the limited seismic bandwidth and low signal-to-noise ratio of the actual seismic data set (on average the signal-to-noise ratio is 1.8 in the reservoir layer along the section).

We first apply the inversion at the well location and invert the inverted seismic attributes obtained from the collocated seismic trace. The prior distribution is the same as in the previous examples, whereas the covariance matrix of the error is assumed to be diagonal with variances equal to 10% of the mean of the actual measurements. Because of the lower resolution of seismic data compared with well-log data, the conditioning data show a smoother behavior, as presented in Figure 13. For this reason, the estimated posterior probability of porosity, clay volume, and water saturation show a larger uncertainty (Figure 14) than the corresponding results conditioned by well-log data (Figure 8). The standard deviation of porosity is reduced by 18%, the standard deviation of clay volume by 22%, and the standard deviation of water saturation by 21%. The interquartile ranges of posterior marginal distributions are 0.16 for porosity, 0.29 for clay volume, and 0.57 for water saturation. As expected, water saturation is the most uncertain property. Indeed the corresponding 90% confidence interval almost covers the entire range of saturation values. However, we notice that all three properties are correctly estimated, within a certain tolerance, in the main reservoir layer.

We finally compare the Bayesian inversion results by using the exact rock-physics model and the linearized approximation. Because the exact rock-physics model is nonlinear, an analytical solution is not available. We therefore discretize the model parameter and data ranges and numerically evaluate the likelihood function for each possible combination of the discretized variables and then

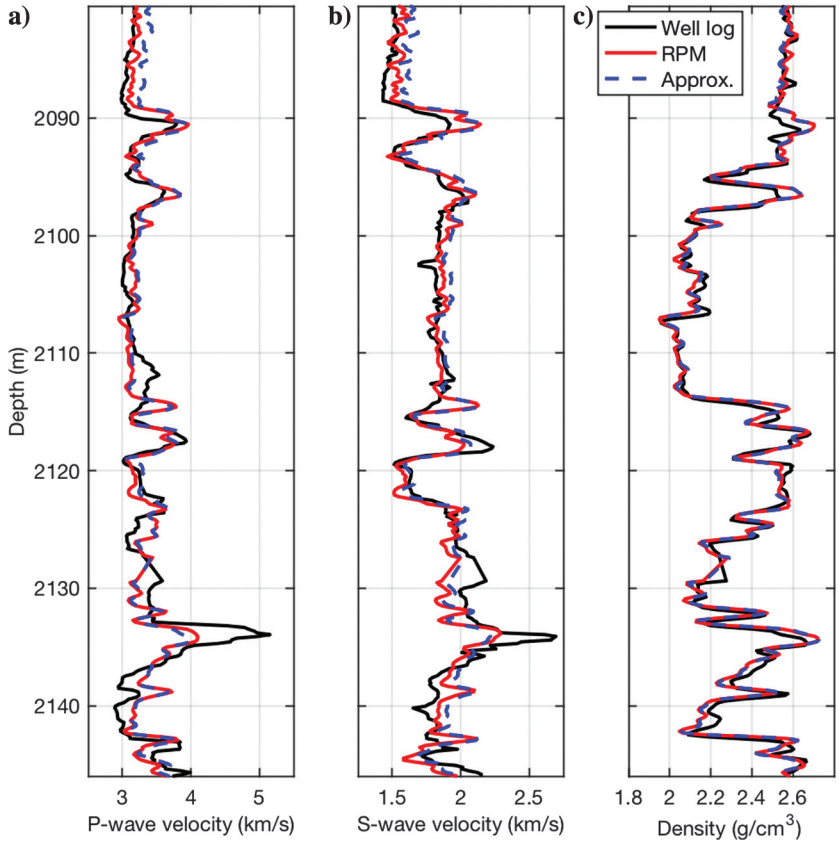

Figure 9. Rock-physics model approximation (stiff sand model). (a) P-wave velocity, (b) S-wave velocity, and (c) density (black curves represent the actual well log, red curves represent the rock-physics model predictions, and dashed blue curves represent the linearized model predictions).

numerically compute the posterior distribution. The results are almost identical (Figure 15). The correlations between exact and linearized inversion results for porosity, clay content, and water saturation are 0.94, 0.89, and 0.91, respectively.

DISCUSSION

This work introduces a mathematical approach for the linearization of the rock-physics model and adopts an analytical Bayesian approach under Gaussian assumptions of the parameters distributions. In general, rock-physics models are not linear, but the nonlinearity is not strong. Indeed, the model calibration plots in the examples show that the models used in this work are almost linear with respect to the model parameters. The advantage of the current approach is that the linearization of the models allows us to derive analytical solutions of the rock-physics inverse problem. In our application, we adopted the Bayesian approach to estimate the model parameters and their uncertainty. However, least-squares inversion methods and regularized approaches (Aster et al., 2011) could be used as well with the presented linearized model. The proposed approach can be directly integrated in the Bayesian linearized AVO inversion proposed by Buland and Omre (2003); however, because the Bayesian AVO approach assumes a log-normal distribution of the elastic properties, to combine this approach with the linearized rock-physics inversion, the rock-physics linearization should be performed in the logarithmic domain.

An example of a model where the linearization in terms of porosity might fail is the soft sand model for highly unconsolidated sand, because of the nonlinear behavior of the model due to the harmonic average formulation. In this case, the linearization using Taylor's expansion centered in the mean of the petrophysical properties might introduce a significant bias in the approximation. However, if a facies classification is available, it is possible to introduce a piecewise linearization, where, in each facies, we compute a new linearization of the rock-physics model. An example of this approach is shown in Figure 2 for Raymer's model. A similar example, where the linearization in terms of saturation might fail, is a rock-physics model in which we assume a homogeneous saturation law for a gas-water mixture. Homogeneous mixtures are common for reservoir fluids. A nonlinear rock-physics model should be used in these situations.

The current approach can be extended to other elastic attributes, such as P- and S-impedances and Poisson's ratio, by introducing additional derivatives, using the chain rule. Similarly, other rock and fluid properties, such as calcite volume, gas, or oil saturation, can be estimated as long as a suitable rock-physics model is available. Additional rock-physics relations can be also included in the

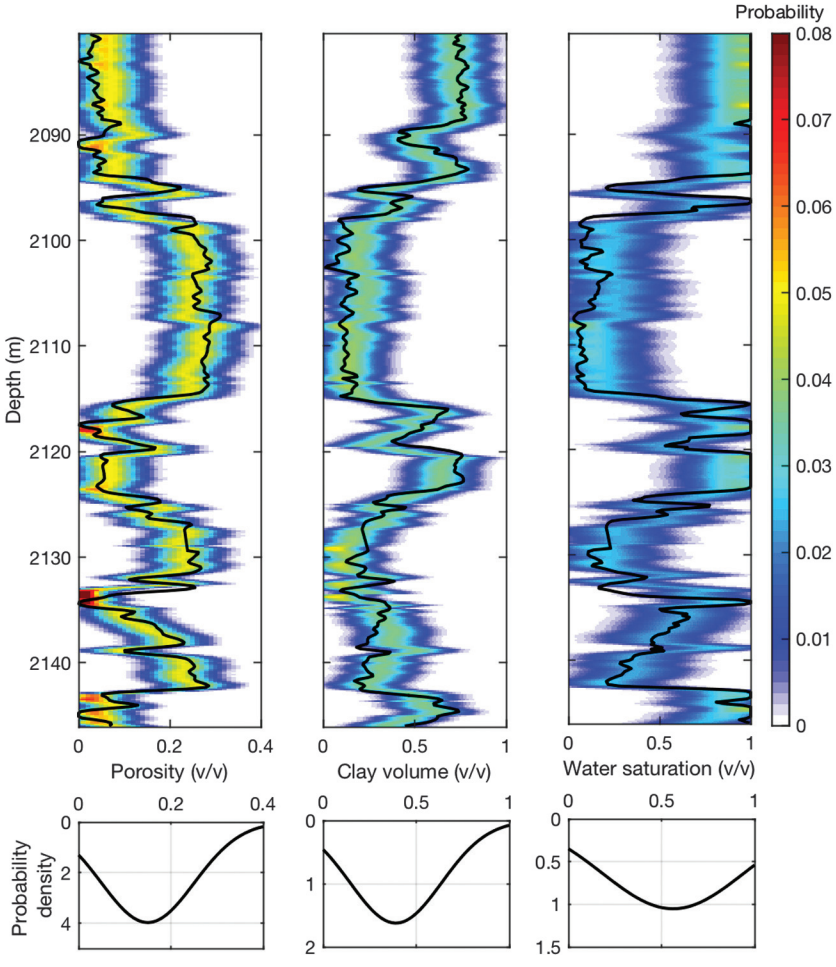

Figure 10. Rock-physics model inversion of elastic-log data (stiff sand model). From left to right: posterior probability distributions of porosity, clay volume, and water saturation (black lines represent the actual well data, and the background color represents the posterior probability distribution). The bottom plots show the prior marginal distributions of porosity, clay volume, and water saturation, respectively.

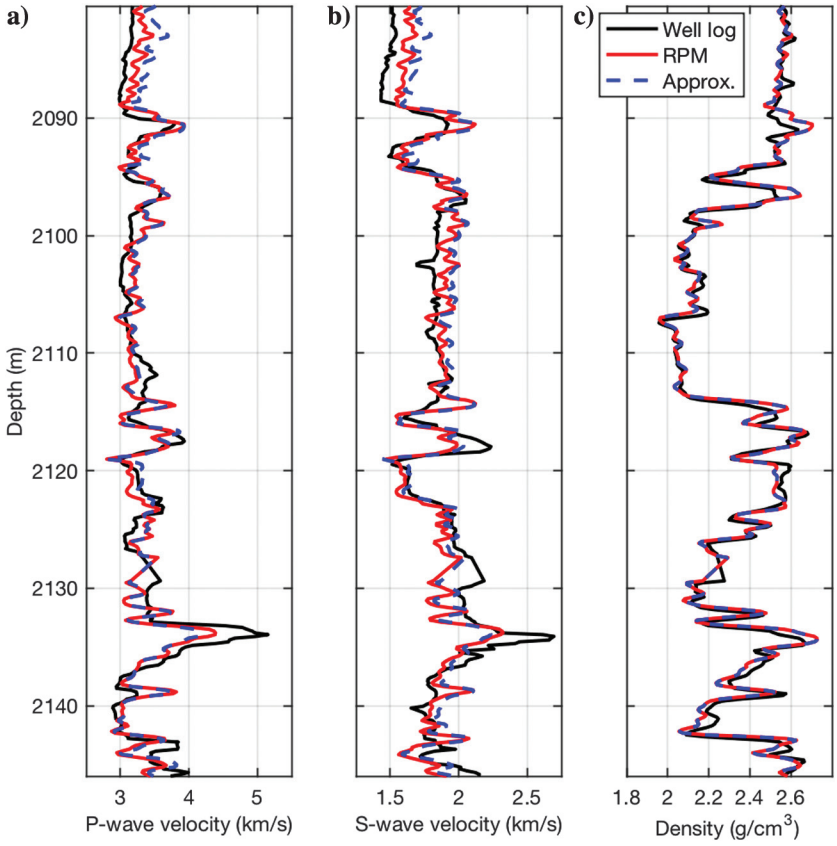

Figure 11. Rock-physics model approximation (inclusion model). (a) P-wave velocity, (b) S-wave velocity, and (c) density (black curves represent the actual well log, red curves represent the rock-physics model predictions, and dashed blue curves represent the linearized model predictions).

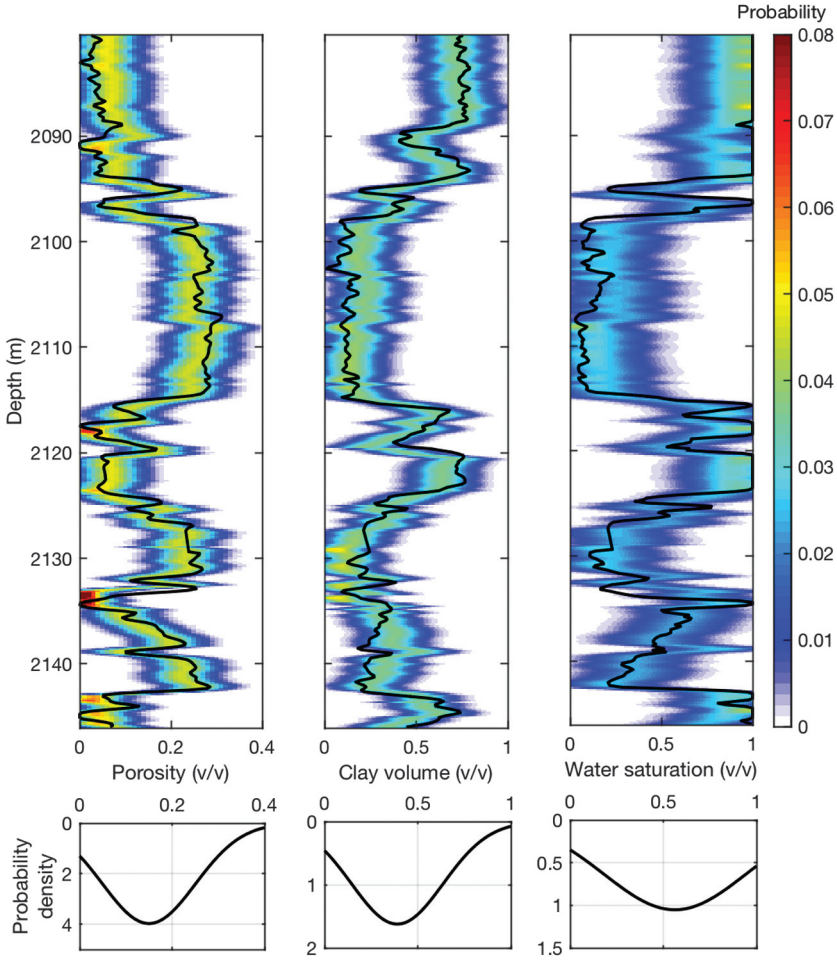

Figure 12. Rock-physics model inversion of elastic-log data (inclusion model). From left to right: posterior probability distributions of porosity, clay volume, and water saturation (black lines represent the actual well data, and the background color represents the posterior probability distribution). The bottom plots show the prior marginal distributions of porosity, clay volume, and water saturation, respectively.

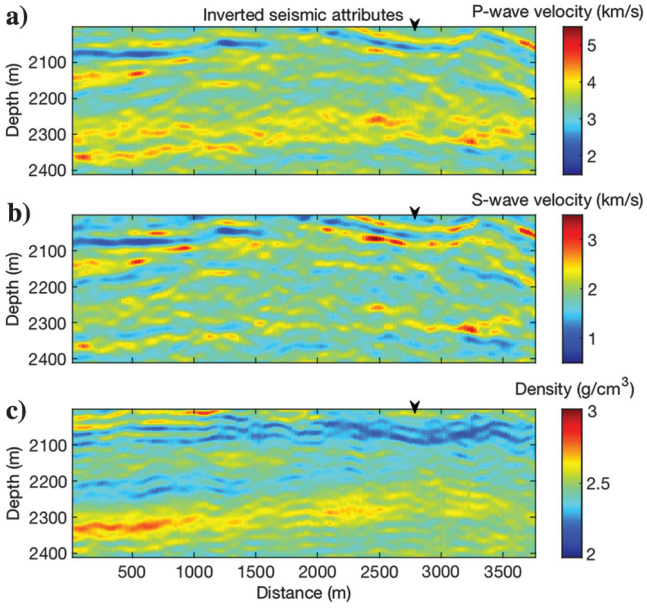

Figure 13. Set of 2D sections of elastic attributes used as conditioning data in the rock-physics inversion. (a) P-wave velocity, (b) S-wave velocity, and (c) density. The black triangle indicates the well location.

inversion workflow. For example, Archie, Simandoux, or Poupon-Leveaux equations could be introduced to improve the fluid estimation. Because these models include exponential relations, the logarithm of the model response should be first computed to estimate the model linearization.

This work focuses on the model linearization and the inverse problem formulation. The inversion in the proposed examples was presented, assuming a Gaussian distribution of the petrophysical properties. However, petrophysical properties are generally not Gaussian. Analytical formulations of the Bayesian approach for skewed and multimodal distributions are presented in Rimstad and Omre (2010) and Grana and Della Rossa (2010), respectively, and could be used for the rock-physics inversion. When the data are not Gaussian, for skewed distributions, normal score transformations can be introduced as well. For multimodal distributions, the normal score transformation has some limitations; therefore, we suggest to model each mode independently and then linearly combine the distributions according to a set of weights, such as the facies proportions.

Most of the examples presented in this work are based on well-log data. However, the inversion can be applied to elastic attributes estimated from seismic data at the well location and in the entire reservoir volume as shown in the last example. The extension of the inversion to the 3D model is not computationally demanding. Indeed, in the Gaussian case, once a rock-physics model has been

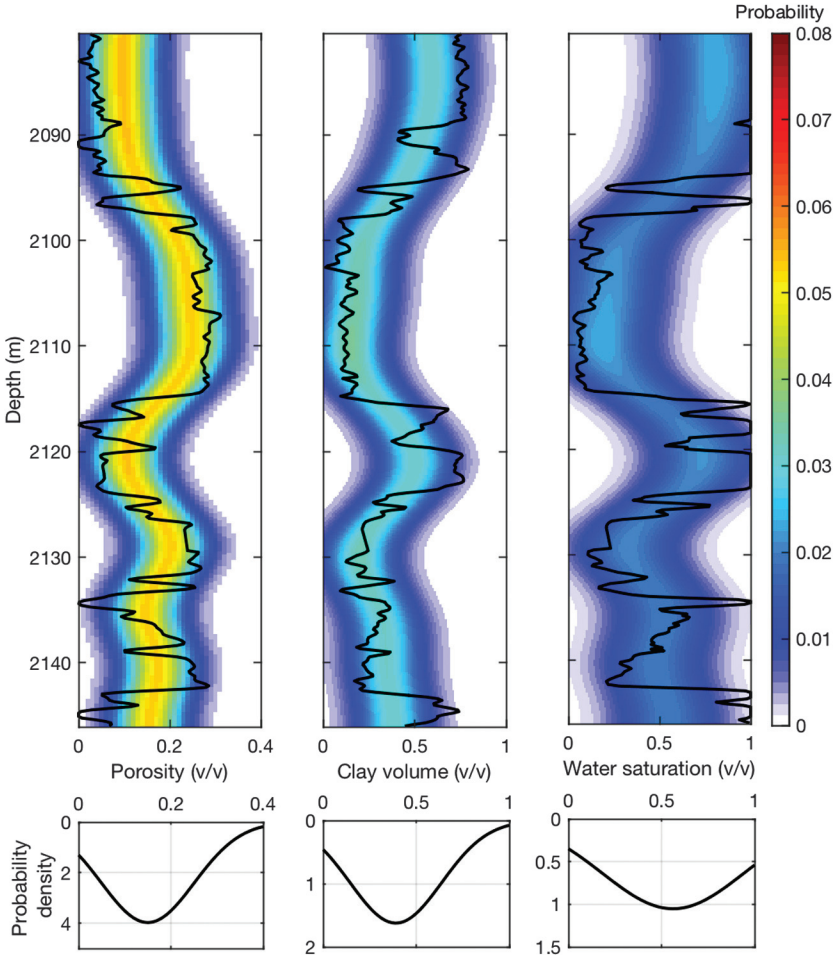

Figure 14. Rock-physics model inversion of collocated inverted seismic trace (position 2750 m in Figure 13). From left to right: posterior probability distributions of porosity, clay volume, and water saturation (black lines represent the actual well data, and the background color represents the posterior probability distribution). The bottom plots show the prior marginal distributions of porosity, clay volume, and water saturation, respectively.

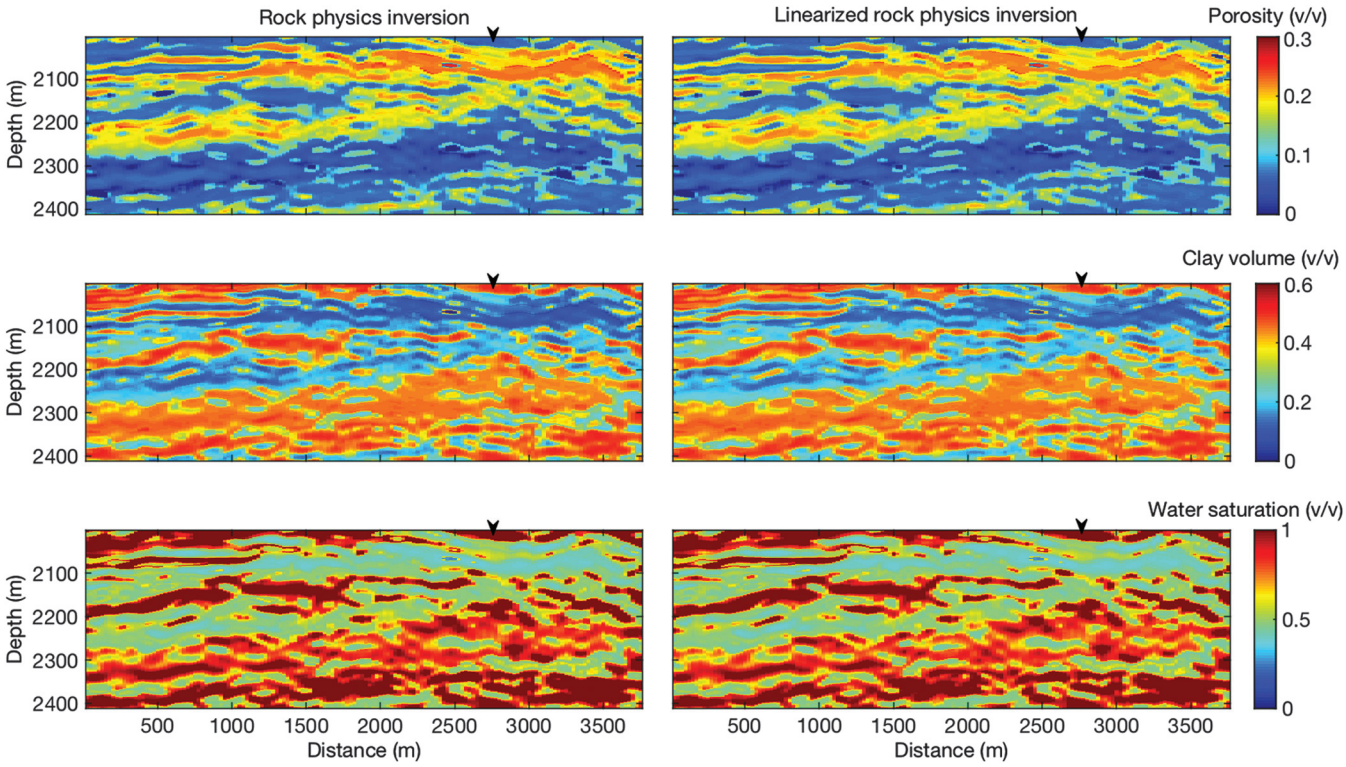

Figure 15. Bayesian rock-physics inversion of elastic properties in Figure 9 for petrophysical properties: porosity (top), clay volume (middle), and water saturation (bottom). Plots on the left show the inversion results using the exact rock-physics model, and plots on the right show the inversion results using the linearized model. The black triangle indicates the well location.

calibrated at the well location, the inversion only requires the computation of the conditional mean and the spatially independent covariance matrix at each location in the seismic grid (equations 7 and 8). However, we point out that the rock-physics inversion in the seismic grid assumes that the rock-physics model calibrated at the well location is also valid far away from the well. Furthermore, the resolution of the inverted seismic attributes (i.e., the conditioning data in the rock-physics inversion) is lower than the well-log resolution. Because of the lower resolution of seismic data, misclassifications at the seismic scale occur more frequently, especially in thin layers below the seismic resolution. Several methods have been proposed to account for the resolution aspect in the inversion. If a Bayesian linearized AVO inversion is applied for the elastic inversion of partial stacked seismic data, and the proposed Bayesian linearized rock-physics inversion is applied for the petrophysical property prediction from seismic attributes, then the so-obtained probability distributions can be combined using the probabilistic upscaling method based on the Chapman-Kolmogorov equation proposed in Grana and Della Rossa (2010). However, this approach might fail in highly anisotropic geologic environments, such as thin layers and fractures, for the nonlinearity of the geophysical relations governing the upscaling.

CONCLUSION

We have presented an analytical formulation of the rock-physics inversion workflow based on a Bayesian approach to the inverse problem. The formulation relies on the Gaussian assumption of the model to be estimated and on the linearization of the rock-physics model. The linearized rock-physics model is obtained by calculating the first-order approximation of Taylor's series expansion. Because the rock-physics model depends on the lithologic environment, we proposed the linearized formulation of three different rock-physics models: the empirical Raymer's model, the stiff sand model based on granular media theory, and the Kuster-Toksöz model based on inclusion theory. The method is applicable to rock-physics models that are linear or slightly nonlinear, but might fail for highly nonlinear models. The explicit analytical form of the posterior distribution provides a computationally fast-inversion method. The examples using well-log data show that all inverted parameters are correctly estimated, when the rock-physics model provides accurate predictions.

ACKNOWLEDGMENTS

The author acknowledges the School of Energy Resources and the Department of Geology and Geophysics of the University of Wyoming for their support. The author also acknowledges A. Buland (Statoil) for the helpful comments and suggestions.

APPENDIX A

RAYMER MODEL PARTIAL DERIVATIVES

The partial derivatives of P-wave velocity with respect to the model parameters (first row of the Jacobian matrix) are

$$\frac{\partial V_P}{\partial \phi} = -2(1-\phi)V_{P,mat} + V_{P,fl}, \tag{A-1}$$

$$\frac{\partial V_P}{\partial C} = (1-\phi)^2 \frac{1}{V_{P,mat}} \frac{\psi_P \rho_{mat} - M_{mat}(\rho_c - \rho_q)}{(\rho_{mat})^2}, \tag{A-2}$$

where

$$\psi_P = \frac{1}{2}\left((K_c - K_q) - \left(\frac{1/K_c - 1/K_q}{(C/K_c + (1-C)/K_q)^2}\right)\right) + \frac{2}{3}\left((G_c - G_q) - \left(\frac{1/G_c - 1/G_q}{(C/G_c + (1-C)/KG_q)^2}\right)\right), \tag{A-3}$$

$$\frac{\partial V_P}{\partial S_w} = \phi \frac{1}{2V_{P,fl}} \frac{(K_w - K_{hc})\rho_{fl} - K_{fl}(\rho_w - \rho_{hc})}{(\rho_{fl})^2}. \tag{A-4}$$

The partial derivatives of S-wave velocity with respect to the model parameters (second row of the Jacobian matrix) are

$$\frac{\partial V_S}{\partial \phi} = -2(1-\phi)V_{S,mat}\sqrt{\frac{(1-\phi)\rho_{mat}}{\rho}} + (1-\phi)^2 V_{S,mat} \frac{1}{2\sqrt{\frac{(1-\phi)\rho_{mat}}{\rho}}} \frac{-\rho_{mat}\rho_{fl}}{\rho^2}, \tag{A-5}$$

$$\frac{\partial V_S}{\partial C} = (1-\phi)^2 \left(\frac{1}{2V_{S,mat}} \frac{\psi_S \rho_{mat} - G_{mat}(\rho_c - \rho_q)}{\rho_{mat}^2} \sqrt{\frac{(1-\phi)\rho_{mat}}{\rho}} + V_{S,mat} \frac{1}{2\sqrt{\frac{(1-\phi)\rho_{mat}}{\rho}}} \frac{(1-\phi)(\rho_c - \rho_q)\phi\rho_{fl}}{\rho^2}\right) \tag{A-6}$$

where

$$\psi_S = \frac{1}{2}\left((G_c - G_q) - \left(\frac{1/G_c - 1/G_q}{(C/G_c + (1-C)/KG_q)^2}\right)\right), \tag{A-7}$$

$$\frac{\partial V_S}{\partial S_w} = (1-\phi)^2 V_{S,mat} \frac{1}{2\sqrt{\frac{(1-\phi)\rho_{mat}}{\rho}}} \frac{-\phi(\rho_w - \rho_{hc})(1-\phi)\rho_{mat}}{\rho^2}, \tag{A-8}$$

The partial derivatives of density with respect to the model parameters (third row of the Jacobian matrix) are

$$\frac{\partial \rho}{\partial \phi} = -\rho_{mat} + \rho_{fl}, \tag{A-9}$$

$$\frac{\partial \rho}{\partial C} = (1-\phi)(\rho_c - \rho_q), \tag{A-10}$$

$$\frac{\partial \rho}{\partial S_w} = \phi(\rho_w - \rho_{hc}). \tag{A-11}$$

APPENDIX B

STIFF SAND MODEL PARTIAL DERIVATIVES

To compute the derivative with respect to porosity, we first rewrite the rock-physics model equations (equations 23–25) by regrouping all the terms that do not depend on porosity. The saturated-rock bulk modulus can be then written as

$$K_{sat} = \frac{K_{mat}\left(\alpha + \frac{4}{3}G_{mat}\beta\phi + \gamma\right)}{\alpha - K_{mat}\beta\phi + \gamma}, \tag{B-1}$$

where

$$\alpha = K_{fl}M_{mat}(K_{mat} - K_{HM}), \tag{B-2}$$

$$\beta = (K_{mat} - K_{HM})(K_{fl} - K_{mat}), \tag{B-3}$$

$$\gamma = K_{mat}\left(\frac{4}{3}G_{mat} + K_{HM}\right)(K_{mat} - K_{fl})\phi_c, \tag{B-4}$$

and the saturated-rock shear modulus is

$$G_{sat} = \frac{\phi(G_{HM} - G_{mat})\xi + \delta G_{mat}}{\phi(G_{mat} - G_{HM}) + \delta}, \tag{B-5}$$

where

$$\delta = (\xi + G_{HM})\phi_c. \tag{B-6}$$

The rock-physics model predictions are then obtained by combining the velocity definitions (equations 26 and 27) with the so-obtained expressions of the elastic moduli (equations B-1–B-6) and the density relation.

The derivatives of P- and S-wave velocities with respect to porosity are then

$$\frac{\partial V_P}{\partial \phi} = \frac{1}{2\rho^2 V_P}\left(\rho\left(\frac{\beta(\alpha+\gamma)K_{mat}M_{mat}}{(\alpha - K_{mat}\beta\phi + \gamma)^2} + \frac{4}{3}\frac{\delta(G_{HM} - G_{mat})(G_{mat} + \xi)}{(\phi(G_{mat} - G_{HM}) + \delta)^2}\right) - M_{sat}(\rho_{fl} - \rho_{mat})\right), \tag{B-7}$$

$$\frac{\partial V_S}{\partial \phi} = \frac{1}{2\rho^2 V_S}\left(\rho\left(\frac{\delta(G_{HM} - G_{mat})(G_{mat} + \xi)}{(\delta - (G_{HM} - G_{mat})\phi)^2}\right) - G_{sat}(\rho_{fl} - \rho_{mat})\right). \tag{B-8}$$

The derivative of density with respect to porosity is the same as in equation A-9.

Similarly, to compute the derivatives with respect to water saturation, we first rewrite the model in a compact form and regroup all the terms that do not depend on the fluid bulk modulus (i.e., on water saturation). The shear modulus does not depend on the fluid; therefore, its derivative with respect to water saturation is zero. The expression for the saturated-rock bulk modulus is

$$K_{\text{sat}} = \frac{K_{\text{mat}}\left(K_{\text{fl}}\left(\eta + \frac{4}{3}\theta G_{\text{mat}} - \lambda\right) + K_{\text{mat}}\left(\lambda - \frac{4}{3}\theta G_{\text{mat}}\right)\right)}{K_{\text{fl}}(\eta - \theta K_{\text{mat}} - \lambda) + K_{\text{mat}}(\lambda + \theta K_{\text{mat}})}, \tag{B-9}$$

where

$$\eta = (K_{\text{mat}} - K_{\text{HM}})M_{\text{mat}}, \tag{B-10}$$

$$\theta = (K_{\text{mat}} - K_{\text{HM}})\phi, \tag{B-11}$$

$$\lambda = \left(\frac{4}{3}G_{\text{mat}} + K_{\text{HM}}\right)K_{\text{mat}}\phi_c. \tag{B-12}$$

Clearly, the expressions in equations B-1 and B-9 are exactly the same; we simply regrouped the terms depending on porosity (equation B-1) and fluid bulk modulus (equation B-9) to simplify the illustration of the computation of the Jacobian. We then compute the derivatives of P- and S-wave velocities with respect to water saturation:

$$\frac{\partial V_{\text{P}}}{\partial S_w} = \frac{1}{2\rho^2 V_{\text{P}}}\left(\rho\left(\frac{\eta\theta(K_w - K_{hc})(K_{\text{mat}})^2 M_{\text{mat}}}{(\eta K_{\text{fl}} - (K_{\text{fl}} - K_{\text{mat}})(\lambda + \theta K_{\text{mat}}))^2}\right) - M_{\text{sat}}\phi(\rho_w - \rho_{hc})\right), \tag{B-13}$$

$$\frac{\partial V_{\text{S}}}{\partial S_w} = -\frac{1}{2\rho^2 V_{\text{S}}}G_{\text{sat}}\phi(\rho_w - \rho_{hc}). \tag{B-14}$$

The derivative of density with respect to water saturation is the same as in equation A-11.

APPENDIX C

INCLUSION MODEL PARTIAL DERIVATIVES

The derivatives of P- and S-wave velocities with respect to porosity and water saturation are

$$\frac{\partial V_{\text{P}}}{\partial \phi} = \frac{1}{2\rho^2 V_{\text{P}}}\left(\rho\left(\frac{(4G_{\text{mat}} + 3K_{\text{fl}})(K_{\text{fl}} - K_{\text{mat}})(4G_{\text{mat}} + 3K_{\text{mat}})}{(4G_{\text{mat}} + 3K_{\text{fl}} - 3K_{\text{fl}}\phi + 3K_{\text{mat}}\phi)^2} + \frac{20G_{\text{mat}}(32G_{\text{mat}}^2 + 60K_{\text{mat}}G_{\text{mat}} + 27K_{\text{mat}}^2)}{3\ (9K_{\text{mat}} + 8G_{\text{mat}} + 6(K_{\text{mat}} + 2G_{\text{mat}})\phi)^2}\right) - M_{\text{sat}}(\rho_{fl} - \rho_{\text{mat}})\right), \tag{C-1}$$

$$\frac{\partial V_{\text{P}}}{\partial S_w} = \frac{1}{2\rho^2 V_{\text{P}}}\left(\rho\left(\frac{(K_w - K_{hc})(4G_{\text{mat}} + 3K_{\text{mat}})^2\phi}{(4G_{\text{mat}} + 3K_{\text{fl}} - 3K_{\text{fl}}\phi + 3K_{\text{mat}}\phi)^2}\right) - M_{\text{sat}}\phi(\rho_w - \rho_{hc})\right), \tag{C-2}$$

$$\frac{\partial V_{\text{S}}}{\partial \phi} = \frac{1}{2\rho^2 V_{\text{S}}}\left(\rho\left(\frac{-5G_{\text{mat}}(32G_{\text{mat}}^2 + 60K_{\text{mat}}G_{\text{mat}} + 27K_{\text{mat}}^2)}{(9K_{\text{mat}} + 8G_{\text{mat}} + 6(K_{\text{mat}} + 2G_{\text{mat}})\phi)^2}\right) - G_{\text{sat}}(\rho_{\text{fl}} - \rho_{\text{mat}})\right), \tag{C-3}$$

$$\frac{\partial V_{\text{S}}}{\partial S_w} = -\frac{1}{2\rho^2 V_{\text{S}}}G_{\text{sat}}\phi(\rho_w - \rho_{hc}). \tag{C-4}$$

The derivatives of density with respect to porosity and water saturation are given in equations A-9 and A-11.

REFERENCES

Aki, K., and P. G. Richards, 1980, Quantitative seismology: W. H. Freeman &Co.

Aster, R. C., B. Borchers, and C. H. Thurber, 2011, Parameter estimation and inverse problems: Elsevier.

Atkinson, K. A., 1989, An introduction to numerical analysis: Wiley.

Avseth, P., T. Mukerji, and G. Mavko, 2005, Quantitative seismic interpretation: Cambridge University Press.

Bachrach, R., 2006, Joint estimation of porosity and saturation using stochastic rock-physics modeling: Geophysics, **71**, no. 5, O53–O63, doi: 10.1190/1.2235991.

Bornard, R., F. Allo, T. Coléou, Y. Freudenreich, D. H. Caldwell, and J. G. Hamman, 2005, Petrophysical seismic inversion to determine more accurate and precise reservoir properties: SPE Europec/EAGE Annual Conference, SPE 94144.

Bosch, M., C. Carvajal, J. Rodrigues, A. Torres, M. Aldana, and J. Sierra, 2009, Petrophysical seismic inversion conditioned to well-log data: Methods and application to a gas reservoir: Geophysics, **74**, no. 2, O1–O15, doi: 10.1190/1.3043796.

Buland, A., and Y. El Ouair, 2006, Bayesian time-lapse inversion: Geophysics, **71**, no. 3, R43–R48, doi: 10.1190/1.2196874.

Buland, A., and O. Kolbjørnsen, 2012, Bayesian inversion of CSEM and magnetotelluric data: Geophysics, **77**, no. 1, E33–E42, doi: 10.1190/geo2010-0298.1.

Buland, A., O. Kolbjørnsen, and A. J. Carter, 2011, Bayesian Dix inversion: Geophysics, **76**, no. 2, R15–R22, doi: 10.1190/1.3552596.

Buland, A., O. Kolbjørnsen, R. Hauge, O. Skjæveland, and K. Duffaut, 2008, Bayesian lithology and fluid prediction from seismic prestack data: Geophysics, **73**, no. 3, C13–C21, doi: 10.1190/1.2842150.

Buland, A., O. Kolbjørnsen, and H. Omre, 2003, Rapid spatially coupled AVO inversion in the Fourier domain: Geophysics, **68**, 824–836, doi: 10.1190/1.1581035.

Buland, A., and H. Omre, 2003, Bayesian linearized AVO inversion: Geophysics, **68**, 185–198, doi: 10.1190/1.1543206.

Coléou, T., F. Allo, R. Bornard, J. Hamman, and D. Caldwell, 2005, Petrophysical seismic inversion: 75th Annual International Meeting, SEG, Expanded Abstracts, 1355–1358.

Doyen, P., 2007, Seismic reservoir characterization: EAGE.

Dvorkin, J., 2008, Yet another V_S equation: Geophysics, **73**, no. 2, E35–E39, doi: 10.1190/1.2820604.

Dvorkin, J., M. Gutierrez, and D. Grana, 2014, Seismic reflections of rock properties: Cambridge University Press.

Dvorkin, J., A. Nur, and H. Yin, 1994, Effective properties of cemented granular materials: Mechanics of Materials, **18**, 351–366, doi: 10.1016/0167-6636(94)90044-2.

Eidsvik, J., P. Avseth, H. Omre, T. Mukerji, and G. Mavko, 2004, Stochastic reservoir characterization using prestack seismic data: Geophysics, **69**, 978–993, doi: 10.1190/1.1778241.

González, E. F., T. Mukerji, and G. Mavko, 2008, Seismic inversion combining rock physics and multiple-point geostatistics: Geophysics, **73**, no. 1, R11–R21, doi: 10.1190/1.2803748.

Grana, D., and E. Della Rossa, 2010, Probabilistic petrophysical-properties estimation integrating statistical rock physics with seismic inversion: Geophysics, **75**, no. 3, O21–O37, doi: 10.1190/1.3386676.
Gunning, J., and M. Glinsky, 2007, Detection of reservoir quality using Bayesian seismic inversion: Geophysics, **72**, no. 3, R37–R49, doi: 10.1190/1.2713043.
Han, D., 1986, Effects of porosity and clay content on acoustic properties of sandstones and unconsolidated sediments: Ph.D. thesis, Stanford University.
Hansen, T. M., A. G. Journel, A. Tarantola, and K. Mosegaard, 2006, Linear inverse Gaussian theory and geostatistics: Geophysics, **71**, no. 6, R101–R111, doi: 10.1190/1.2345195.
Hörmander, L., 1990, The analysis of partial differential operators: Springer.
Johansen, T. A., E. H. Jensen, G. Mavko, and J. Dvorkin, 2013, Inverse rock physics modeling for reservoir quality prediction: Geophysics, **78**, no. 2, M1–M18, doi: 10.1190/geo2012-0215.1.
Kuster, G. T., and M. N. Toksöz, 1974, Velocity and attenuation of seismic waves in two-phase media: Geophysics, **39**, 587–606, doi: 10.1190/1.1440450..
Larsen, A. L., M. Ulvmoen, H. Omre, and A. Buland, 2006, Bayesian lithology/fluid prediction and simulation on the basis of a Markov-chain prior model: Geophysics, **71**, no. 5, R69–R78, doi: 10.1190/1.2245469.
Mavko, G., T. Mukerji, and J. Dvorkin, 2009, The rock physics handbook: Cambridge University Press.
Mazzotti, A., and E. Zamboni, 2003, Petrophysical inversion of AVA data: Geophysical Prospecting, **51**, 517–530, doi: 10.1046/j.1365-2478.2003.00389.x.
Mukerji, T., A. Jørstad, P. Avseth, G. Mavko, and J. R. Granli, 2001, Mapping lithofacies and pore-fluid probabilities in a North Sea reservoir: Seismic inversions and statistical rock physics: Geophysics, **66**, 988–1001, doi: 10.1190/1.1487078.
Raymer, L. L., E. R. Hunt, and J. S. Gardner, 1980, An improved sonic transit time-to-porosity transform: Transactions of SPWLA, Paper P.
Rimstad, K., and H. Omre, 2010, Impact of rock-physics depth trends and Markov random fields on hierarchical Bayesian lithology/fluid prediction: Geophysics, **75**, no. 4, R93–R108, doi: 10.1190/1.3463475.
Russell, B., 1988, Introduction to seismic inversion methods: SEG.
Sen, M. K., and P. L. Stoffa, 2013, Global optimization methods in geophysical inversion: Cambridge University Press.
Spikes, K., T. Mukerji, J. Dvorkin, and G. Mavko, 2007, Probabilistic seismic inversion based on rock-physics models: Geophysics, **72**, no. 5, R87–R97, doi: 10.1190/1.2760162.
Stewart, J., 2015, Multivariable calculus: Nelson Education.
Tarantola, A., 2005, Inverse problem theory: SIAM.
Ulvmoen, M., and H. Omre, 2010, Improved resolution in Bayesian lithology/fluid inversion from prestack seismic data and well observations: Part 1 — Methodology: Geophysics, **75**, no. 2, R21–R35, doi: 10.1190/1.3294570.
Ursin, B., and A. Stovas, 2006, Traveltime approximations for a layered transversely isotropic medium: Geophysics, **71**, no. 2, D23–D33, doi: 10.1190/1.2187716.